EXPERIMENTAL CHARACTERISATION OF A SWEEPING JET ACTUATOR TO CONTROL TURBULENT SEPARATED FLOWS

Tocquer Mathieu
Université d'Orléans, INSA-CVL
PRISME EA 4229
8 rue Léonard de Vinci, Orléans, F45072
mathieu.tocquer@univ-orleans.fr

Raibaudo Cédric
Université d'Orléans, INSA-CVL
PRISME EA 4229
8 rue Léonard de Vinci, Orléans, F45072
cedric.raibaudo@univ-orleans.fr

Kourta Azeddine
Université d'Orléans, INSA-CVL
PRISME EA 4229
8 rue Léonard de Vinci, Orléans, F45072
azeddine.kourta@univ-orleans.fr

ABSTRACT

The present study aims to investigate a developed sweeping jet (SWJ) actuator to control separated turbulent flows to improve the aerodynamic performances of transport vehicles. These fluidic actuators are capable of injecting significant momentum and producing high-frequency oscillations. First, the sweeping jet is experimentally characterised to assess its dynamics, including oscillation frequency f_{osc} and spatial distribution. Subsequently, eight SWJ actuators are applied to a 25° angle ramp to mitigate turbulent flow separation. Wall pressure measurements are used to estimate the drag of the ramp. The results indicate a drag reduction when the actuation angles are set at 30° and 45°. Two-dimensional, two-component Particle Image Velocimetry (2D2C PIV) measurements show a reduction of the recirculation bubble by up to 50% with low-pressure control and complete suppression with higher pressure. The mechanism explaining the control phenomenon is that the streamwise and shear stresses of the Reynolds stress tensor are intensified by the control, leading to an enhancement of the mixing in the separated shear layer and consequently to a reduction of the recirculation length.

INTRODUCTION

The occurrence of flow separation poses a challenge for various aerodynamic applications, leading to notable decrease of aerodynamic performances. Suppressing or at least decreasing separation has become a focal point to improve aerodynamics. For instance, during takeoff, aircraft often encounter difficulties in generating sufficient lift at steep angles of attack due to the appearance of separation on suction side of the wings. To enhance lift in such conditions, the current approach consists on adding to a wing geometry flaps and slats along both leading and trailing edges. However, this modification introduces a considerable increase in the aircraft's weight and hence a drag. The consequence is the increase of the fuel consumption and also the occurrence of a material robustness problem. An alternative approach is to act directly on the flow to improve aerodynamic performances. One method is to use passive control, achieved by integrating small obstacles or roughness elements into the geometry. Vortex generators for example are a widely used tool to control flow separation Godard & Stanislas (2006). These devices energise the boundary layer, enhancing its ability to withstand adverse pressure gradients by generating counter-rotating vortices near the surface. While this technique may degrade control performance in specific flow scenarios, it proves highly effective when applied under planned flow conditions. A more effective approach is to use active control systems capable of adapting to varying flow conditions. This adaptability has shown considerable promise in recent decades due to its ability to respond to changing flow dynamics. Active actuators, such as fluidic oscillators and pulsed-jet mechanisms, are used for this purpose (Wang *et al.* (2016); Raibaudo *et al.* (2017)). However, for these actuators to significantly impact aerodynamics, they need to operate at high frequencies and impart high momentum to the flow (Cattafesta & Sheplak (2011); Viard *et al.* (2020)).

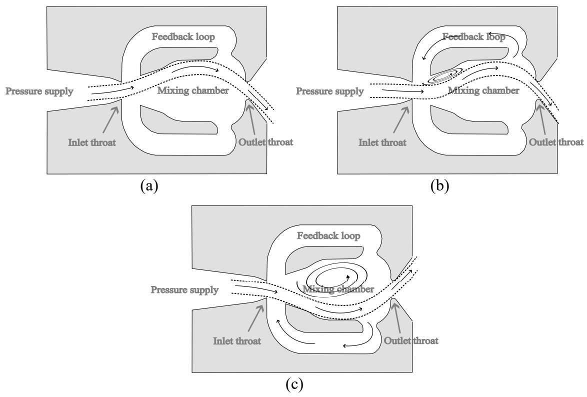

Figure 1. Working principle of the sweeping jet actuator. (a) Coanda phase, (b) feedback phase and (c) switching phase.

Recently, the sweeping jet actuator has received considerable attention among active control actuators. With its unique feature of pressure injection and absence of moving parts, it can induce high-frequency oscillations and inject high momentum. These characteristics have found applications in various domains, such as enhancing the performance of land vehicles (Veerasamy *et al.* (2022); Khan *et al.* (2022)), underwater vehicles (Schmidt *et al.* (2017)), and aircraft wings (Woszidlo & Wygnanski (2011); Childs *et al.* (2016); Andino *et al.* (2015)). Moreover, sweeping jets have been used to mitigate side effects of flow separation such as vibration and noise (Raman & Raghu, 2004). The SWJ employs a three-step behaviour to induce oscillatory motion at the outlet. The operating concept is shown in Fig. 1. Initially, the inlet flow enters the mixing chamber and, adheres to either the top or bottom surface due to the Coanda effect. Consequently, the outlet jet is redirected in the opposite direction (Fig.1a). Subsequently, a segment of the flow traverses through the corresponding feedback loop, inducing recirculation at the inlet throat (Fig.1b). As the recirculation area expands, the primary flow is gradually pushed on the opposite side of the mixing chamber, causing the outlet flow to be deflected in the opposite direction (Fig. 1c). This process repeats cyclically.

For the control application, the characterisation of the interaction between SWJs and the main flow is needed. This can be addressed by investigating how SWJs influence the flow using a well documented case, the flow over the ramp (Stella *et al.* (2017); Kourta *et al.* (2015)). This case presents a separated turbulent shear layer with recirculation at a fixed point in the flow (the leading edge of the ramp), this geometry has been categorised into three distinct regions.

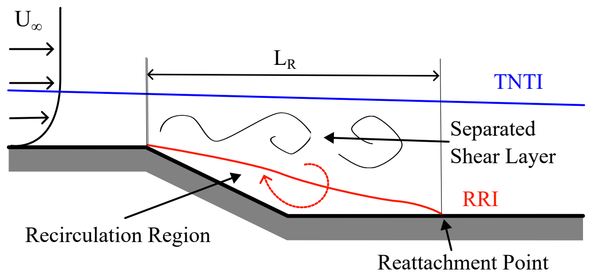

Figure 2. Schematic of a turbulent separated shear layer over a ramp.

The primary flow is positioned away from the ramp and is characterised by minimal turbulence and a positive mean streamwise velocity. The interface between turbulent and non-turbulent flow (turbulent-non-turbulent interface TNTI), depicted by the blue line (Fig.2), delineates this area. The interface of the recirculation region (recirculation region interface RRI) (illustrated by the red line in Fig.2) defines the region of recirculation, situated downstream of the leading edge and adjacent to the ramp. Its key features include low turbulence levels and a negative mean streamwise velocity. Between the TNTI and the RRI lies a separated shear layer characterised by positive mean streamwise velocity and heightened turbulence. This region exhibits complex and unsteady physics (e.g. Kelvin-Helmholtz instabilities), marked by a wide range of time and length scales (Aubrun *et al.* (2000); Kourta *et al.* (2015)).

The objective of this study is twofold: first, to characterise the flow produced by a sweeping jet for potential application in flow control, and second, to improve our understanding and to better characterise the interaction between a separated turbulent shear layer and sweeping jet actuators (SWJs). To achieve this, the experimental setups are first outlined, discussing both the setups themselves and the measurement techniques employed. Subsequently, the findings of the sweeping jet characterisation are presented. These jets are utilised to mitigate separation over a 25° slope ramp. The mean properties of the controlled flow, such as the drag coefficient and recirculation length, are first examined to evaluate the effectiveness of the control method. Subsequent sections are dedicated to explain the control mechanism through Particle Image Velocimetry (PIV) measurements and an analysis of the Reynolds stress tensor. At the end of this paper conclusions and perspectives are provided.

EXPERIMENTAL SET-UP

In this study, two experimental setups are used. One is used to examine and assess the SWJ characterisation and the other one to study the flow control.

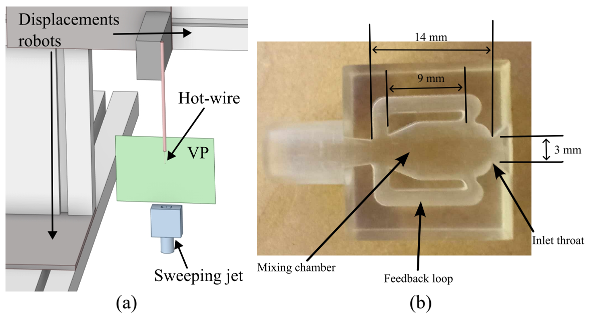

Figure 3. Experimental setup for SWJ characterisation. (a) Platform used for the actuator characterisation. (b) Dimension of the actuator.

The PRISME laboratory in Orléans, France's Flow Control Actuators experimental platform was used to characterise the SWJ geometry chosen in this study and is presented in Fig. 3a. The platform is equipped with a 55P11 hot-wire probe for monitoring the flow velocity generated by the SWJ. With an accuracy of 0.1 mm, the sensor can be moved in three directions by three ISEL displacement robots. This allows to study the propagation of the jet wake over a large area. The Dantec Dynamics Stream Ware software controls the position of the hot wire and the velocity acquisition. The measurement plan is then shown in Fig. 3a. It is comparable to a vertical plan (VP) positioned in the center of the jet. The range of interest is $15H \times 20H$, and $\frac{1}{6}H \leq \Delta_{Y,Z} \leq 1H$. To ensure the convergence of the mean and the standard deviation of the signal, the sampling frequency is $F_s = 60$ kHz, and the acquisition time is $T_s = 2$ s for each spatial point. This corresponds to at least 1000 oscillation periods for the lowest oscillation frequency that was tested. A manometer is connected to the SWJ to measure the inlet pressure P_0. The flow rate Q is measured using a flowmeter upstream of the valve.

The shape of the SWJ used is presented in Fig. 3b. The SWJ is printed using a Fromlabs Form 2 SLA 3D printer with a resolution of 25 μm. It has a 3 mm-wide nozzle H. It consists of a mixing chamber with a throat-to-throat length of $L_{osc} = 14$ mm and two 9 mm-long feedback pathways that permit a part of the main flow to recirculate. In this work, nine relative inlet pressures P_0 between 20 and 100 kPa are tested, corresponding to a flow rate ranging from $0.9e^{-3}$ to $1.3e^{-3}$ $m^3.s^{-1}$ (or 1.3 to 3 $g.s^{-1}$).

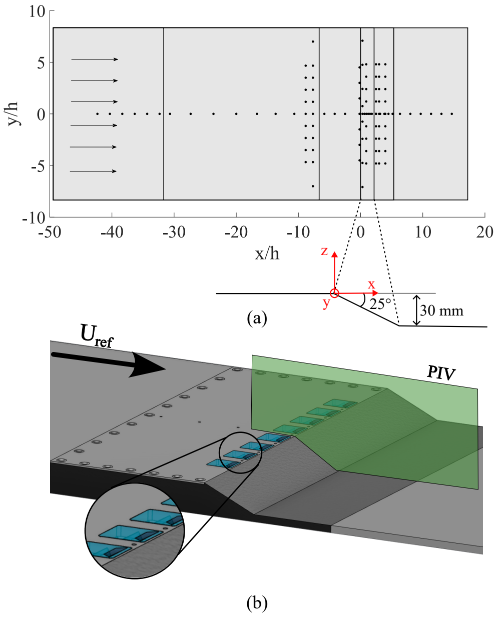

Figure 4. Experimental setup of the ramp geometry and the metrology. (a) Distribution of the pressure measurements. Black dots correspond to pressure taps. (b) Geometry of the ramp with implemented SWJs.

The second test bench is the ramp with an angle $\beta = 25°$ and a height of $h = 30$ mm, located inside the test section of 50×50 cm^2 and 2 m long of the S2 Eiffel open wind tunnel of the PRISME Laboratory in Orléans. Eight SWJ actuators are installed on the ramp. Actuators are pitched at three different angles of 30, 45, and 90°. The ramp used is identical to the one examined in the study by Stella *et al.* (2017) and is presented in Fig. 4. 103 wall pressure sensors are placed on the ramp (Fig. 4a). The pressure is recorded using two MPS4000 pressure scanners with a sampling frequency of 500 Hz, and it is synchronised with particle image velocimetry (PIV) measurements in the centre line of the ramp. 2D2C planar PIV is used with a sampling frequency of 4 Hz and a spatial resolution of 11.89 px/mm (84 $\mu m/px$). To do so, one 11 Mpx camera with a 50 mm focal length is used in order to cover a field of view of $8h \times 3h$. 2000 pairs of images are taken to ensure the convergence of the results. This corresponds to a total acquisition time of 500 s. In this study, the free-stream velocity U_∞ used is respectively 15, 20, and 25 $m.s^{-1}$ and PIV measurements are taken for an actuation angle of 30° and a free-stream velocity of 20 $m.s^{-1}$. 7 different inlet pressures inside the actuators are tested to highlight the efficiency of the SWJ in controlling the separation over the ramp ($P_0 = 0; 1; 3; 5; 13; 15; 18$ kPa).

RESULTS

SWJ characterisation

The SWJ is characterised in terms of temporal and spatial evolution. Fig. 5a shows the oscillation frequency of the produced jet with respect to the input pressure. The trend is linear for low inlet pressure ($P_0 \leq 10$ kPa). For the pressure range tested, the oscillation frequency reaches a maximum around 2200 Hz for high pressures. Compared to other bi-stable oscillators tested in the laboratory (Wang et al. (2016)), where ($f_{osc} \approx 500$ Hz), SWJ achieves to perform higher frequencies, which will be a valuable asset for the control of turbulent separated flows.

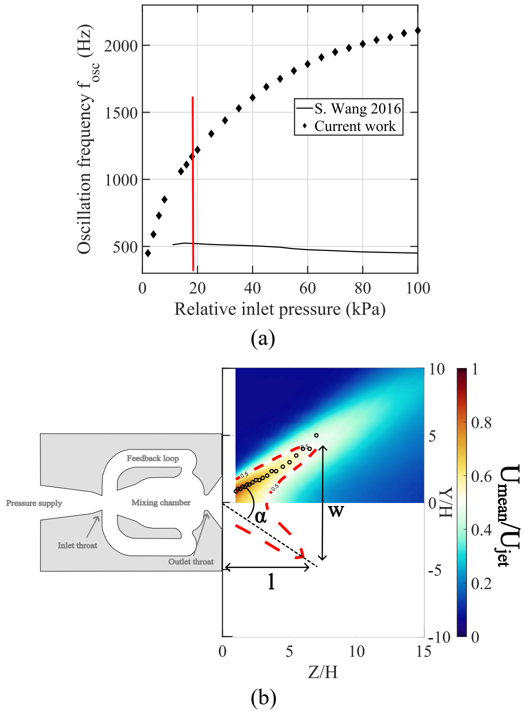

Figure 5. Spatio-temporal characterisation of the sweeping jet. (a) Evolution of oscillation frequency. (red line) shows the maximum of pressure used in this study for control application. (b) Spatial distrubution of the jet flow for an inlet pressure $P_0 = 20$ kPa. (red line) corresponds to the threshold used to define the jet geometry.

In this study, only low inlet pressures are used to control the separated flow of the ramp. This corresponds to a maximum oscillation frequency of about 1200 Hz, as presented by the red line in Fig. 5a.

The mean wake topology of the produced flow is presented in Fig. 5b. The threshold used is based on a criterion defined by Ostermann *et al.* (2018); it corresponds to half of the reference velocity inside the SWJ (as shown with the red line in Fig. 5b). The jet created has the shape of a butterfly. It provides information about the jet's residence time inside the actuator during the switching mechanism. For every oscillation period, the jet spends more time on the sidewalls of the SWJ's mixing chamber due to the presence of high velocity zones on both sides of the jet (Fig. 5b), creating a bi-stable flow at the outlet. A more in-depth description of the flow produced by this SWJ can be found here Tocquer *et al.* (2024).

Turbulent separation flow control

Estimation of the drag coefficient In order to state the effectiveness of the SWJ to control separated flows, the pressure drag coefficient C_D is estimated using wall pressure measurements for all tested cases.

$$C_D = -\int_{ramp} C_P cos(\beta) dl \quad (1)$$

With C_P the pressure coefficient at the wall estimated using pressure measurements. The integral is calculated on the descending part of the ramp and is projected on the streamwise axes. Figure 6 shows the evolution of the drag coefficient with the momentum coefficient C_μ for the three actuation angles tested. In this study, the momentum coefficient is given by:

$$C_\mu = \frac{\rho_{jet} U_{jet}^2 A_{jet}}{\frac{1}{2}\rho_\infty U_\infty^2 S_{ramp}} \quad (2)$$

Where U_{jet} is the jet velocity calculated using the flow rate inside the actuators, ρ_{jet} is the density estimated with isentropic calculation, and A_{jet} is the total exit area of the 8 actuators. ρ_∞ and U_∞ are the density and the velocity of the flow, and S_{ramp} is calculated using the ramp height h and the section of the wind tunnel.

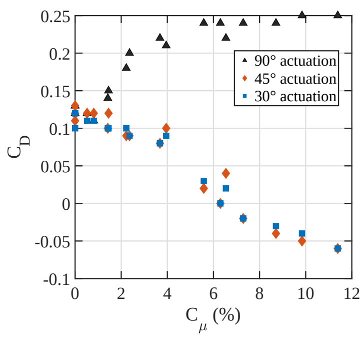

Figure 6. Pressure drag coefficient C_D with the momentum coefficient for different angles of actuation.

With an actuation angle of 90°, the drag coefficient is increased for almost all tested pressures. It only displays some benefits for the lowest inlet pressure tested, where the C_D goes from 0.12 to 0.11, corresponding to a ΔC_D of 5.7 %. For other two angles of actuation, the evolution of the drag coefficient is the same. It decreases slowly for low momentum coefficients $C_\mu \leq 2$ %, where $\Delta C_{Dmax} = 24$ % for a 45° actuation angle and $C_\mu = 1.42$ %. Then the C_D decreases with a higher rate for higher C_μ up to a full recovery of the drag $\Delta C_D \approx 100$ % at $C_\mu \approx 6$ %. SWJs produce net thrust on the ramp for the highest momentum coefficient tested, $C_\mu \geq 6$ % ($\Delta C_D \geq 100$ %).

Impact on the recirculation length The evolution of the recirculation length L_R is related to the effectiveness of the control. The PIV measurements for the SWJ actuation with an angle of 30° are used to calculate the recirculation length by estimating the recirculation region interface (RRI). Where the RRI detection is based on the χ criterion.

Fig. 7 presents the recirculation length for the different flow conditions. During the increase of C_μ, the SWJ flow is first incompressible and becomes compressible for higher C_μ Tocquer *et al.* (2024). During the switching from incompressible case to compressible one, no sweeping of the jet is observed for $4 \leq C_\mu \leq 8$ % in the case where $U_\infty = 20\ m.s^{-1}$. In order to asses data for $4 \leq C_\mu \leq 8$ %, a PIV case is done with $U_\infty = 25\ m.s^{-1}$ and it is represented in red in figure 7.

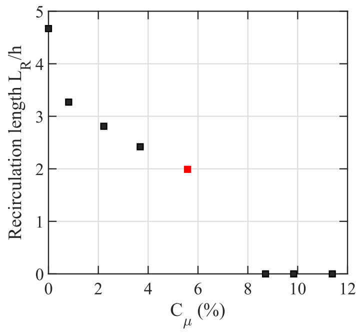

Figure 7. Recirculation length L_R for a 30° angle of actuation. (red dot) correspond to a case with $U_\infty = 25\ m.s^{-1}$.

With increasing momentum coefficients, the length of the recirculation decreases. For $C_\mu \geq 6$ %, it is equal to zero. It also corresponds to the region where the SWJ actuators produce net thrust shown in the previous section.

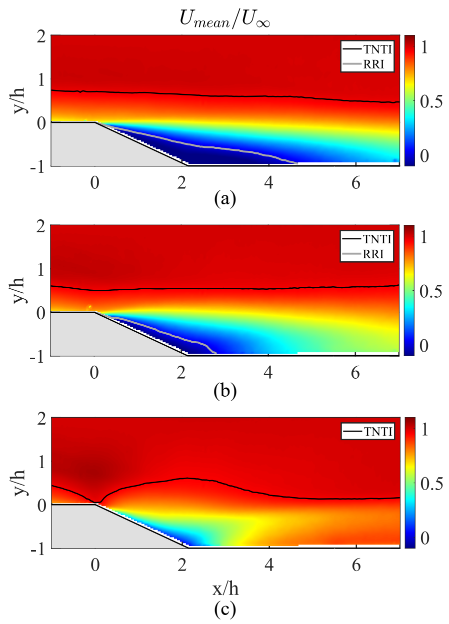

Figure 8. The normalised mean streamwise velocity U_{mean}/U_∞. (a) Baseflow $C_\mu = 0$ %. (b) $C_\mu = 2.22$ %. (c) $C_\mu = 8.71$ %.

Figure 8 displays the mean streamwise velocity over the ramp for the baseflow and two control cases. These corresponds to a momentum coefficient of $C_\mu = 2.22$ % and $C_\mu = 8.71$ % respectively. The mean turbulent-non-turbulent interface (TNTI) and the recirculation region interface (RRI) are plotted in this figure. The TNTI is calculated using a mean velocity threshold based on uniform momentum zones and a detection method used by Kovacs *et al.* (2022). For $C_\mu = 2.22$

%, the recirculation length is reduced, and the shape of the latter is also affected by the control. At $C_\mu = 8.71$ %, it is not possible to clearly detect the separation region. For controlled cases, the high momentum region moves toward the bottom ramp wall (e.g., $x/h \geq 4$ for $C_\mu = 8.71$ %) and the low velocity region is greatly reduced by the control. The turbulent-non-turbulent interface's (TNTI) shape is also modified by the control. All these mechanism induce a modification of the interaction between the separated shear layer and the main flow through the entertainment mechanism.

Analysis of the control effects The control of separated shear flows with SWJs induces a decrease of the recirculation zone by modifying the level of turbulence inside of the controlled flow. Figure 9 shows the turbulent kinetic energy (TKE) k for $C_\mu = 0$, 2.22 and 8.71 %. Where $k = \frac{1}{2}(u'^2 + v'^2 + w'^2)$ and using isotropic hypothesis $w'^2 = \frac{1}{2}(u'^2 + v'^2)$, it becomes $k = \frac{3}{4}(u'^2 + v'^2)$.

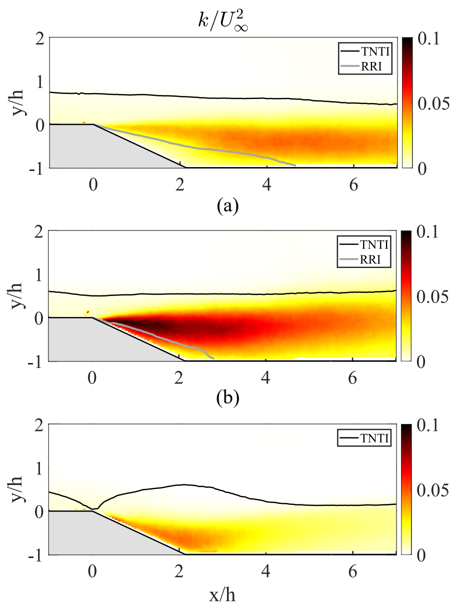

Figure 9. The normalised turbulent kinetic energy k/U_∞^2. (a) Baseflow $C_\mu = 0$ %. (b) $C_\mu = 2.22$ %. (c) $C_\mu = 8.71$ %.

When the SWJs are on, the maximum TKE moves toward the ramp. For the baseflow, the maximum of TKE is located at $x/h \approx 4$. For control cases, it is located at $x/h \approx 1$ and $x/h \approx 2$ for respectively $C_\mu = 2.22$ % and $C_\mu \leq 6$ %. When the SWJ does not generate thrust ($C_\mu \leq 6$ %), the TKE is increased. It is twice compared to the baseflow for $C_\mu = 2.22$ %. Thus, the control with SWJ increases the mixing between the upper and the lower parts of the flow near the ramp, thereby reducing the recirculation length and increasing the pressure on the ramp.

The mechanism for this change can be understood by studying the Reynolds stress tensor. In the following, we will focus on the control case with no thrust production. Fig. 10 and Fig. 11 show the value of the Reynolds stress tensor for both the baseflow and $C_\mu = 2.22$ %.

For the baseflow, the main contribution inside the separated shear flow comes from the streamwise stress (Fig. 10a) with a maximum of $max(|\overline{u'u'}/U_\infty^2|) = 0.0469$. The lowest contribution comes from the shear stress with

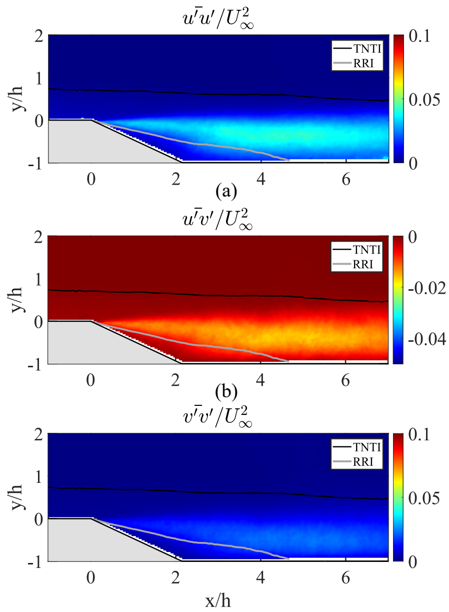

Figure 10. The normalised Reynolds stress tensor for the baseflow $C_\mu = 0$ %. (a) Streamwise stress $\overline{u'u'}/U_\infty^2$. (b) Shear stress $\overline{u'v'}/U_\infty^2$. (c) Normal stress $\overline{v'v'}/U_\infty^2$.

Table 1. Maximum of Reynolds stresses for the baseflow and $C_\mu = 2.22$ %.

	Baseflow	$C_\mu = 2.22$ %
$\max(\lvert\overline{u'u'}/U_\infty^2\rvert)$	0.0469	0.1057
$\max(\lvert\overline{u'v'}/U_\infty^2\rvert)$	0.0169	0.0366
$\max(\lvert\overline{v'v'}/U_\infty^2\rvert)$	0.0247	0.0394

$max(|\overline{u'v'}/U_\infty^2|) = 0.0169$. For the control case, Reynolds stresses move toward the ramp, as same as the TKE, and the streamwise and shear stresses are highly increased, as presented in Fig. 11 and Tab. 1.

Streamwise stress and shear stress are multiplied respectively by 2.5 and 2.2. The contribution of the shear and normal stresses are equivalent for the control case (Tab. 1). The normal stress is also slightly increased, but only near the leading edge of the ramp (Fig. 11c) where the recirculation bubble interacts with the incoming flow.

CONCLUSION AND PERSPECTIVES

Sweeping jets have been proven in the present study to be able to prevent flow separation in terms of mean properties. A first characterisation of the spatio-temporal behaviour of the jet produced by SWJs showed that they can achieve high frequency actuation with moderate inlet pressure. When applied for a flow separation configuration. The actuation angles of 30° and 45° succeeded a reduction of the drag coefficient C_D by up to 24 % for low momentum injection ($C_\mu = 1.42$ %). However, the 90° angle of actuation increased the drag produced by the ramp. Two regimes for the controlled flow have been identified here, depending of the level of momentum coefficient. For the first regime (low momentum coefficients), the control with SWJs leads to a drag reduction and the recirculation length is reduced by more than 50% for the best case. For the other regime, the recirculation is totally suppressed by

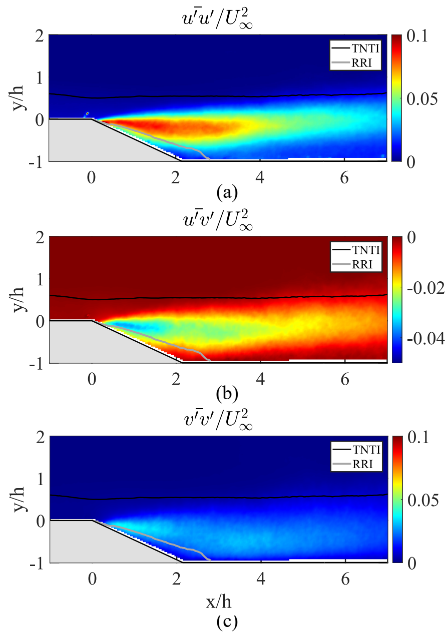

Figure 11. The normalised Reynolds stress tensor for C_μ = 2.22 %. (a) Streamwise stress $\bar{u'u'}/U_\infty^2$. (b) Shear stress $\bar{u'v'}/U_\infty^2$. (c) Normal stress $\bar{v'v'}/U_\infty^2$.

the control, corresponding to higher momentum coefficients ($C_\mu \geq 6$ %) where net thrust is generated by SWJs ($\Delta C_D \geq 100$ %).

Due to the nature of the actuators, the SWJs act on not only the mean but also the turbulent properties of the separated flow. The high momentum region is moved towards the ramp by the control, inducing higher velocity gradients in the streamwise direction. Thus, the production of turbulence is enhanced in this region. This results in an increase in streamwise and shear stresses near the ramp, as well as the turbulent kinetic energy (TKE). Thereby, the mixing between the upper and lower parts of the flow near the ramp is increased, leading to a reduction of the recirculation bubble and an increase in the wall pressure on the ramp. Hence, it decreases the drag.

The mixing between the flow and the recirculation region is affected by this control mechanism, which could be guided by the interaction between the main flow and the separated shear layer through the entrainment mechanism. Therefore, future work will focus on the study of entrainment through the TNTI in control cases.

ACKNOWLEDGEMENT

We would like to gratefully acknowledge the laboratory of Excellence CAPRYSSES framework and the financial support of this study from Grant No. ANR-11-LABX-0006-01 of the Investissements d'Avenir LabEx CAPRYSSES. We would also like to thank Stéphane Loyer for his help during the experiments.

REFERENCES

Andino, M. Y., Lin, J. C., Washburn, A. E., Whalen, E. A., Graff, E. C. & Wygnanski, I. J. 2015 Flow Separation Control on a Full-Scale Vertical Tail Model using Sweeping Jet Actuators. In *53rd AIAA Aerospace Sciences Meeting*. Kissimmee, Florida: American Institute of Aeronautics and Astronautics.

Aubrun, S, Kao, P L & Boisson, H C 2000 Experimental coherent structures extraction and numerical semi-deterministic modelling in the turbulent flow behind a backward-facing step. *Experimental Thermal and Fluid Science* **22**, 93–101.

Cattafesta, L. N. & Sheplak, M. 2011 Actuators for Active Flow Control. *Annual Review of Fluid Mechanics* **43** (1), 247–272.

Childs, R. E., Stremel, P. M., Kushner, L. K., Heineck, J. T. & Storms, B. L. 2016 Simulation of Sweep-Jet Flow Control, Single Jet and Full Vertical Tail. In *54th AIAA Aerospace Sciences Meeting*. San Diego, California, USA: American Institute of Aeronautics and Astronautics.

Godard, G. & Stanislas, M. 2006 Control of a decelerating boundary layer. Part 1: Optimization of passive vortex generators. *Aerospace Science and Technology* **10** (3), 181–191.

Khan, T. I., Tajik, A. R. & Parezanovic, V. 2022 Drag reduction of a generic transport vehicle model using a fluidic oscillator. *International Journal of Thermofluids* **15**, 100180.

Kourta, A., Thacker, A. & Joussot, R. 2015 Analysis and characterization of ramp flow separation. *Experiments in Fluids* **56** (5), 104.

Kovacs, L., Passaggia, P., Mazellier, N. & Lago, V. 2022 Detection method for shock-waves in viscous flows. *Experiments in Fluids* **63** (1), 11.

Ostermann, F., Woszidlo, R., Nayeri, C. N. & Paschereit, C. O. 2018 Properties of a sweeping jet emitted from a fluidic oscillator. *Journal of Fluid Mechanics* **857**, 216–238.

Raibaudo, C., Stanislas, M. & Kerhervé, F. 2017 Transient Characterization of the Reattachment of a Massively Separated Turbulent Boundary Layer Under Flow Control. *Flow, Turbulence and Combustion* **98** (4), 1039–1063.

Raman, G. & Raghu, S. 2004 Cavity Resonance Suppression Using Miniature Fluidic Oscillators. *AIAA Journal* **42** (12), 2608–2612.

Schmidt, H. J., Woszidlo, R., Nayeri, C. N. & Paschereit, C. O. 2017 Separation control with fluidic oscillators in water. *Experiments in Fluids* **58** (8), 106.

Stella, F., Mazellier, N. & Kourta, A. 2017 Scaling of separated shear layers: an investigation of mass entrainment. *Journal of Fluid Mechanics* **826**, 851–887.

Tocquer, M., Raibaudo, C. & Kourta, A. 2024 Experimental characterisation of controlled separated flows using high-frequencies sweeping jets. In *58th 3AF International Conference on Applied Aerodynamics*. Orléans.

Veerasamy, D., Tajik, A. R., Pastur, L. & Parezanović, V. 2022 Effect of base blowing by a large-scale fluidic oscillator on the bistable wake behind a flat-back Ahmed body. *Physics of Fluids* **34** (3), 035115.

Viard, R., Talbi, A., Ghouila-Houri, C., Kourta, A., Merlen, A. & Pernod, P. 2020 Magneto-mechanical micro-valve for active flow control. *Sensors and Actuators A: Physical* **316**, 112387.

Wang, S., Baldas, L., Colin, S., Orieux, S., Kourta, A. & Mazellier, N. 2016 Experimental and Numerical Study of the Frequency Response of a Fluidic Oscillator for Active Flow Control. In *8th AIAA Flow Control Conference*. Washington, D.C.: American Institute of Aeronautics and Astronautics.

Woszidlo, R. & Wygnanski, I. 2011 Parameters Governing Separation Control with Sweeping Jet Actuators. PhD thesis, American Institute of Aeronautics and Astronautics, Honolulu, Hawaii.